

Mutation Effect Generalizability under Selection-Drift

Andre F. Ribeiro¹ (ribeiro@alum.mit.edu)

¹University of Sao Paulo, Sao Carlos, SP, 13560-970, Brazil

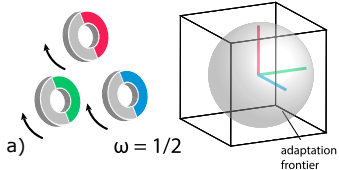
While Neutral Theory famously describes the number of discrete genetic differences in populations, we consider the number of genetic backgrounds under which such differences are observed - setting limits to the generalizability of their effects. This allow us to determine which population structures and diversity rates have maximal effect generalization across (1) environmental and (2) genetic variation, and to demonstrate that they correspond asymptotically to those of populations under (1) natural selection and (2) drift. At the same time, these results suggest distinct limits to the predictability of fitness and evolution across evolutionary regimes. We employ both broad time, large-scale genome sequencing datasets (including whole-genome autocorrelation calculations), and fine time-scale barcoding experiments.

1 Introduction

In complex genomes and environments, the effect of a mutation observed for a population member is rarely the same as that observed for another, due to gene-gene (epistasis) and gene-environment interactions. This could make the selection of beneficial mutations, and natural selection generally, scale poorly under environmental and genomic changes. Increasing evidence points to the shaping influence of mutation robustness (i.e., the external validity of mutation effects across population members) on the evolutionary process¹⁻⁸. Experiments relating selection strength and robustness have offered qualitative-only observations of their relationship, making it difficult to generate new testable predictions, and articulate the relationship between robustness and traditional evolutionary theory. Robustness is typically quantified in simple ways in most studies^{9,10} (e.g., the number of members with overlapping phenotypes in a population), but is related to quickly developing issues of generalization in Machine Learning and Statistics. Theoretically, the relationship between the evolutionary process and robustness¹¹⁻¹⁶, or, the process and arbitrary population-structures¹⁷⁻¹⁹ have remained highly idealized, often accompanied of only simulated or, more commonly, no evidence. Here, we review the theory behind robustness, its relation to adaptation under pleiotropy, and reconsider multiple recent data in light of the resulting model.

We can introduce the problem using Fisher's famous allegory for multi-dimensional adaptation with pleiotropy²⁰⁻²². An individual organism's fitness at an instant is a function of its traits (e.g., body size, beak length), like a microscope's of its knobs' positions. The process of random, and time-extended, adaptation is then analogous to one where we randomly change knob positions, until a sharp image comes through, Fig.1(a). Fitness gains and losses brought by any mutation are, however, contingent on a large number of factors (environmental, developmental, regulatory, etc.) Each observation of fitness is thus valid only in its very instantaneous set of conditions. Since gains from a knob depend on the position of all other knobs, the only sure-way to assure no false-positive

Fisher's Geometric Model (FGM)



Latin-square Model (LSM)

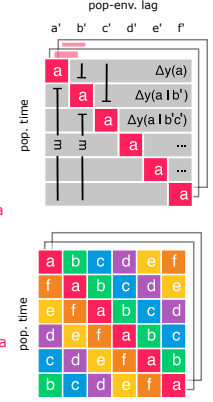
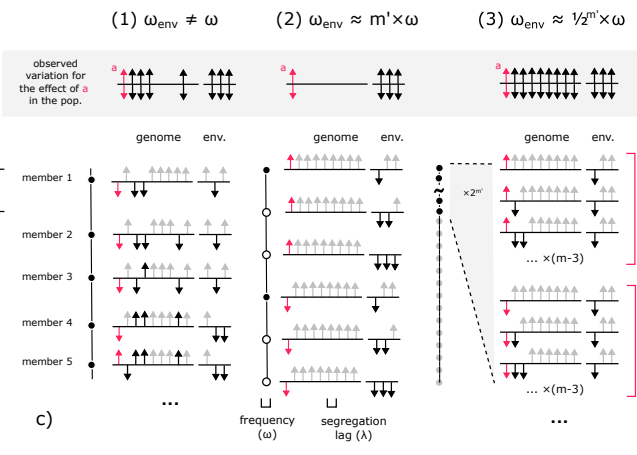
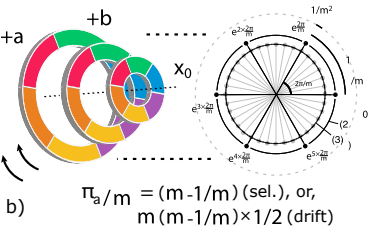


Figure 1 Latin-Square Model (LSM). (a) Fisher's Geometric Model (FGM) and microscope analogy, (b) LSM as a mechanism to generalize mutation effects across populations, (c) population-environment systems (1–3) with rates of change of ω_{env} for the environment and ω for populations, horizontal lines illustrate genomic and environmental variants across population members (rows), arrows show whether they take the same value (up, -1) or alternate (down, $+1$) to a reference x_0 , the gray box shows the range of variation under which the effect of a SNP a is observed, systems' rates of genetic background generation lead to differences in mutation robustness across scenarios, (d) time-extended matrix representations for systems (2) (top) and (3) (bottom).

adaptations is to try each knob position, in each variation of all other knobs. This is illustrated by the wheel in Fig.1(b), which generates all possible knob variations by phasing their rotations. We call this alternative to Fisher’s Geometrical Model (FGM) the Latin-Square Model (LSM).

The FGM is a full randomization approach, where we randomly switch knobs, and approach the instrument non-methodically. The LSM is closer to how a microscope is actually used, where we change a given knob, while systematically fixing all other knobs’ values, in a ’structured randomization’ approach that is akin to simultaneous experimentation. While the FGM makes many assumptions (strong stabilizing selection, equal effect mutations, etc.) the one that washes away issues of robustness is that there are no mutational correlations among traits^{20,22}. In more realistic conditions, moving a knob would move many other knobs, in unknown ways. The microscope’s design, like the experimental, is an apt abstraction because it breaks down all possible variations available to its operator in dimensions whose effects remain unconfounded throughout adaptation. Exactly because of this assumption of independence, Fisher was able to model adaptation as trajectories in a Euclidean m -dimensional space, finally showing that adaptation largely takes place in a sphere around the optimal, Fig.1(a). In both models, FGM and LSM, mutation effects are commutable. In Fisher’s model, this requires a statistical independence assumption, while, in the LSM, commutation is afforded by population structure - taken as part of the adaptation process itself. Such questions are fundamental, as they cut to the core of what selection and adaptation are about: populations’ ability to quickly identify the effects of previously unseen, or ’untested’, mutations. As the main source of genomic changes, mutations also play a key role in explaining how populations use genomes to collectively represent (and react to) their environments. This vital population-environment connection has been increasingly de-emphasized with the availability of packaged omnic data, but is formulated explicitly in the LSM.

Populations under external and stationary change. Consider a population in an environment that is changing at a rate of ω_{env} . A critical question for that population is how to choose, in response, its own rate of change ω . Together, the population and environment make up a reciprocal system, where the environment has m' variations, $\{a', b', c', \dots, [m']\}$, that can affect population fitness, $y \in \mathbb{R}$ (where $[m]$ indicates the m -th variant). Throughout this article, we use Latin letters, $\{a, b, c, \dots\}$, to refer to population genetic variations (Single Nucleotide Polymorphisms, SNPs) and primed letters, $\{a', b', c', \dots\}$, to environmental. We also write $+a, -a$ and $\pm a$ for the presence, absence and polymorphism of a in populations. Consider then how populations’ chosen rates, ω , affect their ability to adapt, in particular, in respect to the number and types of effects they observe.

Fig.1(c) illustrates three scenarios

$$(1) \ \omega \neq \omega_{env}, \quad (2) \ m' \times \omega = \omega_{env}, \quad (3) \ 1/2^{m'} \times \omega = \omega_{env}. \quad (1)$$

Genetic variation is illustrated as -1 or $+1$ arrows over individual genomes in a population with m segregating sites (left horizontal lines, values for a reference genome x_0 taken arbitrarily as -1) and n members (rows). Environmental variation is shown similarly in the line to the right. Consider the problem of estimating the effect (on fitness y) of a SNP a . With rates (1) these effects are doubly confounded. Most effect observations $\Delta y(a)$ made in such populations reflect uncontrolled variation in the environment, or concurrent genetic variation. For example, the observed effect on fitness precipitated by population member 1 in Fig.1(c) (first row and column) is the difference $\Delta \hat{y}(a | x_0, +c, +d, +b') = y(x_0 | -a, -b, -c, -d, \dots, -b', -c', -d', \dots) - y(x_0 | +a, -b, +c, +d, \dots, +b', -c', -d', \dots)$. This effect observation reflects not only a 's effect, but also the extraneous variation of (c, d, b') . Using such observations for the selection of a could promote deleterious adaptations, and the increasing accumulation of deleterious epistatic effects.

In contrast, rates (2, 3) lead to population-environment systems where effects are not confounded (and to populations that change at, respectively, slower or faster frequencies than their environments). The gray top-panel in Fig.1(c) depicts all variation under which the effect of SNP a (red) is observed in the previous population, from the individual-level observations in the lower rows. With a frequency of $m' \times \omega_{env}$, we observe the effect $\Delta y(a)$ under every possible environmental variant, $\Delta \hat{y}(a | \pm b', \pm c', \pm d', \dots)$, Fig.1(c, middle). With such per-SNP frequency, the effect of a is appropriately separated from the effect of other SNPs, due to a slow rate of change. Effects in (2) are observed, however, in only one genetic background, $\Delta \hat{y}(a | -b, -c, -d, \dots)$, repeatedly (across all times and populations). Any changes in factors (b, c, d, \dots) , are likely to invalidate these effect observations and, consequently, populations' ability to choose what individual adaptations to promote. We thus say that in (2) effects are unconfounded, but not generalizable across the population. In systems (3), in contrast, each effect $\Delta y(a)$ is observed under full genomic and environmental variation, $\Delta \hat{y}(a | \pm b, \pm c, \pm d, \dots \pm b', \pm c', \pm d', \dots)$, Fig.1(c, right). Any frequencies different from (2) will lead to environmental changes unequally represented in populations (and be 'unbalanced' in the sense of Experimental Designs^{23,24}), and any frequencies different from (3) will lead to genetic changes that not fully generalize across populations. Given the widespread prevalence of epistatic effects among SNPs^{6,25,26}, the generalizability of their effects should be a key factor for adaptation.

Define a quantity $\partial \pi_a / \partial m$ counting the number of effect observations per SNP across populations. The asymptotic limit for this quantity follow directly from the previous rates, Eq.(1),

$$(2) \left\{ \frac{\partial \pi_a}{\partial m} = \left(1 - \frac{1}{m'}\right)^{m'} \rightarrow \frac{1}{e} = 0.36\dots, \quad (3) \left\{ \frac{\partial \pi_a}{\partial m} = \frac{1}{2} \left(m - \frac{1}{m}\right)^{m'} \rightarrow \frac{\phi}{2} = 0.81\dots, \quad (2)$$

which describe the frequency under which effects of a particular SNP are observed every m -time (i.e., per-genome), and ϕ is the golden ratio (m' increasing, m constant). The rate (2) can be thought as: for any new segregating site, make only 1 effect observation for each m variant,

observing the same effect across distinct environmental conditions, Fig.1(c, middle). The per- m rate is $m \times (1 - 1/m) = (m - 1/m)$ in this case, Eq.(1). The rate for (3) can be thought as: for each new site, also observe effects for all other $m - 1$ sites, and $(m - 1/m)$ positions every m time.* The per- m rate for a fixed a value is $m \times (m - 1/m)$ in this case (i.e., m times the previous). These two rates express opposite conditions for effect observations, where they are observed under none or all possible genetic backgrounds. With a fixed number of segregating sites, m , these two rates lead, in turn, to known asymptotic expressions for Euler's number and Fibonacci series rates,† Eq.(2). Alternative proofs are discussed in ²⁴ (Sect. 6 Sample Power), as well as relationships to random sampling and trees.

Population-environment systems with rates (2, 3) in Eq.(1,2) implement the same process, but display different segregation and linkage disequilibrium patterns. We will study multiple populations with common size and time of evolution, but either under drift or selection, and demonstrate that their background diversity rates correspond to, respectively, (2) and (3). If the consequent number of effect background observations is a factor on mutation effect generalizability, then we should also observe distinct generalizability patterns in these two evolutionary regimes, across all studied populations. This relationship has been demonstrated in purely statistical grounds²⁴, and is reconsidered bellow for both long and fine time-scale genetic data.

Populations under external and non-stationary change. The definition of mutation robustness implied by the previous discussion is that of robustness as effect invariance. Effect invariance means that whether we make a change a to a population x_i or another x_j , the observed changes in fitness will be identical in both cases, $y(x_i + \{a\}) - y(x_i) = y(x_j + \{a\}) - y(x_j) = \Delta y(a)$, for any $x_i, x_j \subseteq X$ (where X is a set containing all fitness-relevant genetic and environmental factors). Any such measure requires, however, the enumeration of all possible background conditions, x_i , to add a . Systems with rates (2, 3) enumerates all conditions in stationary environments - i.e., with a constant ω_{env} in Eq.(1). Repetition of the same cycles, one for each non-cyclic permutation of environmental variants²⁴, are necessary in non-stationary environments. Systems (2, 3) correspond, therefore, to the only systems where effect invariance for one, (2), or many, (3), mutations can be evaluated and optimized. In them, invariance can be quantified simply by effect observation variance after full background variation, $\text{VAR}^{-1}[\Delta y(a \mid \Pi(X - \{a\}))]$ (where $\Pi(X)$ is the set of all permutations of the elements in X ²⁴). That is, a system is said to be effect-invariant if it is able to **sustain small effect variance under full external variation**. The rates in Eq.(1,2) can thus be seen as generating population structures that maximize invariance, and robustness, under stationary conditions - and an equilibrium position for populations in non-stationary environments.

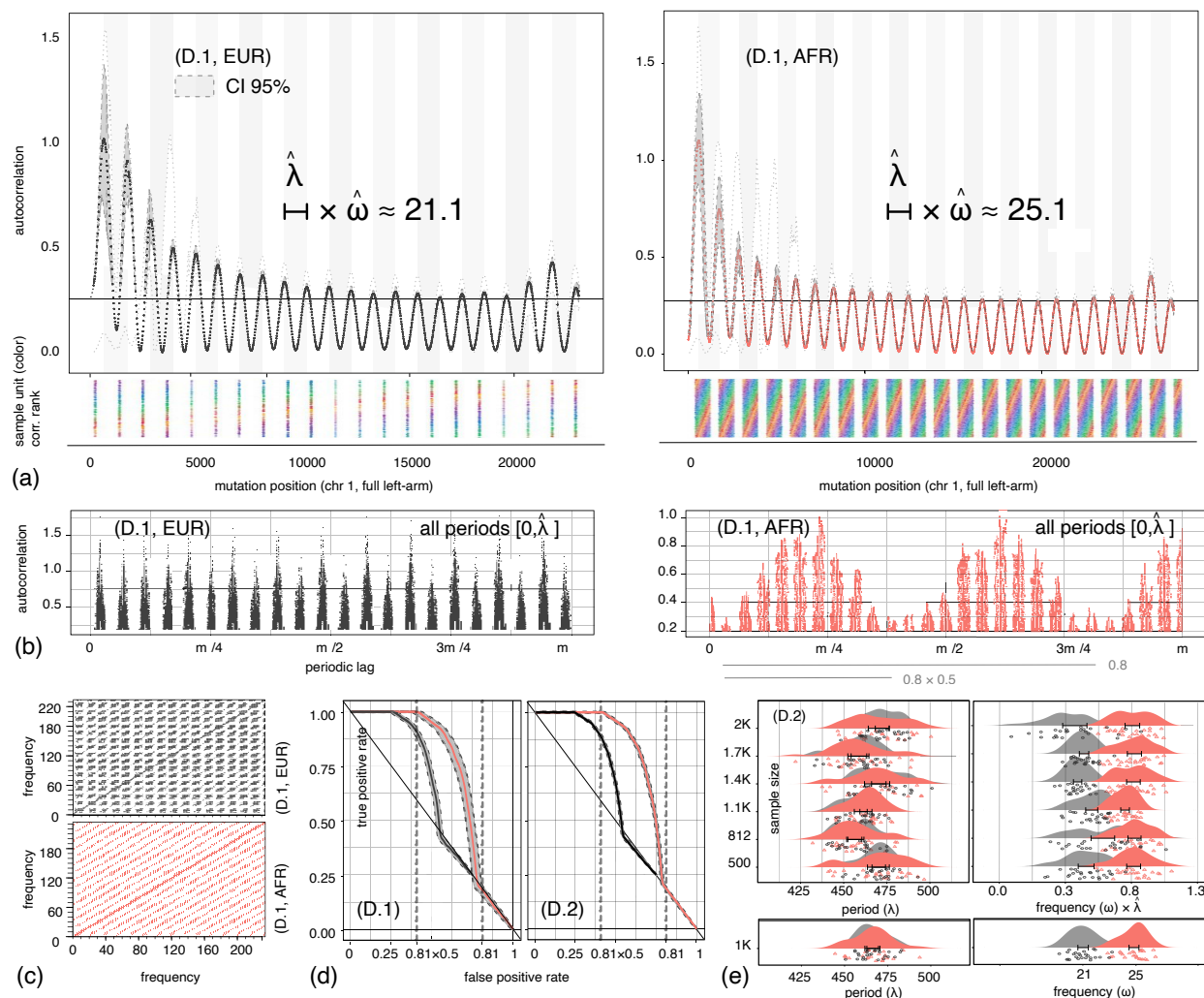


Figure 2 UK Biobank and 1K Genomes (broad time-scale). (a) Autocorrelation $\rho[seg(i)]$ over left-arm of human chromosome 1 across European (EUR, $n = 503$, left) and African (AFR, $n = 661$, right) populations of the 1K Genomes project²⁹ (D.1), gray-white bars show empirical number of cycles per genome, $\hat{\omega}$, and their lag period, $\hat{\lambda}$, autocorrelation confidence intervals (CIs) are shown as dark gray ribbons, **(lower strips)** population (color) correlation rankings across all sites shows periodic correlation, **(b)** genomic periodicities for EUR and AFR populations according to cumulative autocorrelations $\rho[seg(i) - seg(i + l)]$ over all integral lags $0 < l \leq \hat{\lambda}^2$, **(c)** graphical test for periodic correlation, **(c)** SNP survival Empirical ROC curves follow the rates in Eq.(2), **(d)** UK Biobank³⁰ (D.2)'s UK and African born populations (bootstrap with sample sizes of [500, 2000]), **(bottom-row)** have distinct ω but common λ , and, **(top-rows)** distinct periodic components following Eq.(2).

2 Results

The number of genetic differences maintained in populations, π , is a key quantity in **Neutral Theory** (NT)^{31–33}. Under NT, for a constant size (diploid) population at equilibrium with m segregating sites³⁴, $\mathbb{E}[\pi] = \mathbb{E}[m/\sum_{i=1}^{n-1} \frac{1}{i}] = 4N\mu$. Fisher’s Geometric Model (FGM), in turn, has the historical significance of being the first mainstream model to justify the binomial rates observed for genetic differences in populations under no selection pressure, later leading to NT. As expected by NT, rate (3) in Eq.(1) leads to binomial distributions for the number of genetic differences, and selective sweeps with exponential rates, (2), to overdispersed distributions. Unlike these well-know measures of nucleotide and haplotype diversity, we considered the number of possible backgrounds observed for each fixed difference, and interpreted them as counts of SNP effect observations. The consequent patterns in Eq.(2) are patterns over background counts. This characterizes population with a pair $(\pi, \partial\pi_a/\partial m)$ of variables, and leads to counts of partial permutations in populations (*Sect. Combinatorial Enumeration*), and not just their differences. The relationship to **Wright-Fisher** and Moran models of drift are also discussed in the Supporting Material³⁵. In this section, we study how background counts change empirically across evolutionary regimes, and their statistical consequences to populations. Understanding how to predict mutation effects (fitness gains and losses) from environment and genetic conditions has, not only theoretic, but also great practical consequences^{36–38}.

Whole-genome Autocorrelation. We first consider evidence for the LSM using large-scale sequencing datasets, then experimental data. Models of adaptation often consider mutations at a single site, gene or small genome. Mutation rates are, however, a population characteristic, and periodic or multi-scale patterns, like the ones below, are biased, phased, or disappear in genomic segments. Using large-scale computation, we consider combinatorial patterns across thousands of whole-genomes in populations. Fourier and frequency-based representations have been central to many key scientific discoveries (e.g., the DNA double-helix and quantum double-slit experiments). Although the relevance of frequency-based representations to omic data has long been hypothesized^{39,40}, it has led to few empirical results. Genome autocorrelation is a (circular) convolution of the full genome with itself, and indicates across-genome patterns of pairwise overlap and differences - making them useful to demonstrate the previous combinatorial quantities and limits. The conditions in Eq.(2) imply that drift-selection transitions change the frequencies of effect observations, ω , across populations’ genomes, while keeping the separation between segregating sites, λ , constant. These two quantities are illustrated in Fig.1(c, bottom). We say that after the i -th mutation (SNP) in one genome, the population ‘skips’ λ_i previous variants. This implies that the set of segregating positions in each chromosome of a genome can be written as the series $\lambda_0 + \sum_i \lambda_i$, where λ_0 is the skip from the chromosome beginning, and λ_i the subsequent. The case of constant lags is associated with a periodic function over genome positions, $seg(i) = seg(i + \lambda)$, where seg is a binary or integral count variable indicating a segregation at site i . This predicts, in

*the rate (3) is divided by 2 to account for observations with and without a , as required to calculate the effect $\mathbb{E}[\Delta y(a)]$ in populations, and can be calculated in the two cases at rates (2) $2 \times \omega_{env}$ and (3) ω_{env} , Fig.1(c).

†see, for example, ²⁷(Chapter 20) and ²⁸ for simple and illustrated discussions.

turn, periodic autocorrelation functions for each individual chromosome, with constant period λ and frequency ω across population members.

We start with the popular 1000 genomes dataset²⁹ (D.1). Fig.2(a) shows autocorrelation among all SNP positions, $seg(i)$, in the first and largest human chromosome (full left-arm, ~ 0.25 billion SNPs for each individual), across all members of the European (EUR, $n = 503$) and African populations (AFR, $n = 661$). The left-to-right y -values indicate correlations at increasing genomic distances. The gray band shows autocorrelation confidence intervals (CI) among sites, and the dotted line shows the (min-max) range across all population members. These illustrate the strong regularity in correlations across sites, distances, and members. The solid horizontal line marks the baseline rate of $1/4$, indicating the proportion of sites that remain fixed at a time, as expected by NT.

Fig.2(a) also indicates empirical frequencies (i.e., number of cycles per genome), $\hat{\omega}$, and lags, $\hat{\lambda}$, of mutations from all genomes in these populations. The EUR population has gone through the out-of-Africa bottleneck^{41,42} and, unlike the AFR, already underwent the second demographic transition. Multiple genome scans have identified in the past decades differential patterns of selection among these two populations⁴³⁻⁴⁷, and considered the role of novel and diverse environments in this transition^{44,47,48}. Under higher selection pressure (e.g., higher windowed Tajima D values⁴³), the observed number of cycles decreases, while observed lag periods λ remain constant, Fig.2(a). The pattern can be seen in the populations of low-coverage sequencing datasets (D.1) and, even more clearly, in the subpopulations of high-depth datasets. Fig.2(e, bottom-row) shows number of cycles and periods in the African and British-born populations in the UK Biobank³⁰ (D.2, 1000 bootstraps, 6 different sample sizes in $[500, 2000]$) for all chromosomes (and the associated significant results for same λ and different ω hypothesis tests³⁵).

Periodic Correlation. Increased frequency ω , with little change in period λ , leads to periodic correlation across genomes. The notion of correlated periodicity is well-studied⁴⁹, outside genetics. It can be demonstrated in different ways. The colored strips in Fig.2(a, bottom) show population members (each a distinct color) ranked by correlation in each genome position. In periodically correlated systems, variants assume specific correlation levels periodically, one at a time. The strip depicts these across-genome patterns. Fig.2(c) shows graphical tests for correlation periodicity⁵⁰ (D.1). In populations that are periodically correlated, observed frequencies in the test are distributed in equally-spaced diagonals. We observe this (in $\hat{\lambda}$ genome segments) for the AFR, but not EUR, population.

According to the previous, systems (2, 3) differ in their frequency spectra. System (2) is composed of exponential frequencies, and (3) of exponential and fibonaccian frequencies. Fig.2(b) shows cumulative autocorrelations in $seg(i) - seg(i+l)$ vectors, where i are SNP positions³⁵, and, l are all integral lags $l \in [0, \hat{\lambda}]$. This is a common way of revealing periodicities in time-series. The EUR population has regular frequencies at $1/\omega$ intervals every m variants. The AFR population has

a further periodicity: a bisection every $\sim 0.81 \times m$ periods. Both are predicted by the LSM, Eq.(2). Fig.2(e, top-rows) show the same results in the UK Biobank (EUR, AFR). These results further suggest that systems (2, 3) are associated with populations, respectively, under selection, (2), and drift, (3). Distinct rates lead also to distinct autocorrelation patterns across systems, resembling peaks (2) or triangles (3). Practitioners will recognize these patterns, alternating present/absent triangles of same base length, from pairwise LD-block plots^{51,52}. The patterns in Fig.2(b) do not correspond to those patterns, but to their generative source. For example, it is consistently observed that LD-blocks extends over distinct distances in AFR and EUR populations^{53,54}, and that these differences are associated with distinct statistical opportunities (e.g., detect associations in EUR, then perform fine-mapping in AFR^{52,54}).

Mutation Survival and Prediction. In this section, we consider how the previous rates limit the generalizability of mutation effects. Consider two populations with the same founder genome, one under drift and another under selection, evolving during a $[0, t_{max}]$ period. These populations will span distinct combinatorial and statistical landscapes for the selection process. Let $surv_t(x_0 + a)$ be a binary indicator of a SNP a 's survival t generations after its founding mutant. ROC curves are the most common analytical tools to understand the out-of-sample generalizability of algorithms and biological markers, plotting their true-positive (TP) vs. false-positive (FP) rates. The area-under-the-curve for the time-dependent ROC SNP survival curve indicates, in this case,

$$Pr [surv_t(x_0 + a) > surv_t(x_0) \mid y(x_0 + a) > y(x_0), t], \quad (3)$$

and thus selection's ability to rank the true fitness gains in populations after t experimental generations³⁵ (i.e., with high TP rates). An elbow-curve in the ROC diagram, with maximal area and constant TP, describes Darwinian selection (where survival is a reliable indicator of fitness y across mutations). The ROC relationship to natural selection is further discussed in³⁵. Fig.3(a-c, left-column) shows empirical ROC curves for variants in *Saccharomyces cerevisiae*⁵⁶ (D.3, artificial selection, 10 epochs of 100 generations, 2 population replicates), *Drosophila melanogaster*⁵⁷ (D.4, observed high selection in 1 interval, 5 monthly intervals, 10 replicates), and *Escherichia coli*¹ (D.5, artificial selection, 5 generations, 10 replicates) populations. Fig.2(d) shows, in turn, ROC curves with the previous observational datasets, D.1 and D.2, under random sampling.

Under uniform and noiseless selection mechanisms, true positive (TP) rates (y-axis) are associated with effects that are consistent across entire populations (and all possible x_0), Eq.(3). Maintenance of 1.0 TP rates across growing populations in D.3-5 are thus indicative of effect invariance³⁵. In long time-scales, Fig.2(d), effects are invariant under selection until 1/4 of the full sample, which coincide with their level of pairwise fixations. The increased genetic diversity rates under drift increases the number of background conditions in which effects are observed and, consequently, effect invariance for a larger section of the (combinatorially possible) populations. The rate where this transition happens is $\sim 0.81 \times m$, which is the rate necessary, Eq.(2), for vari-

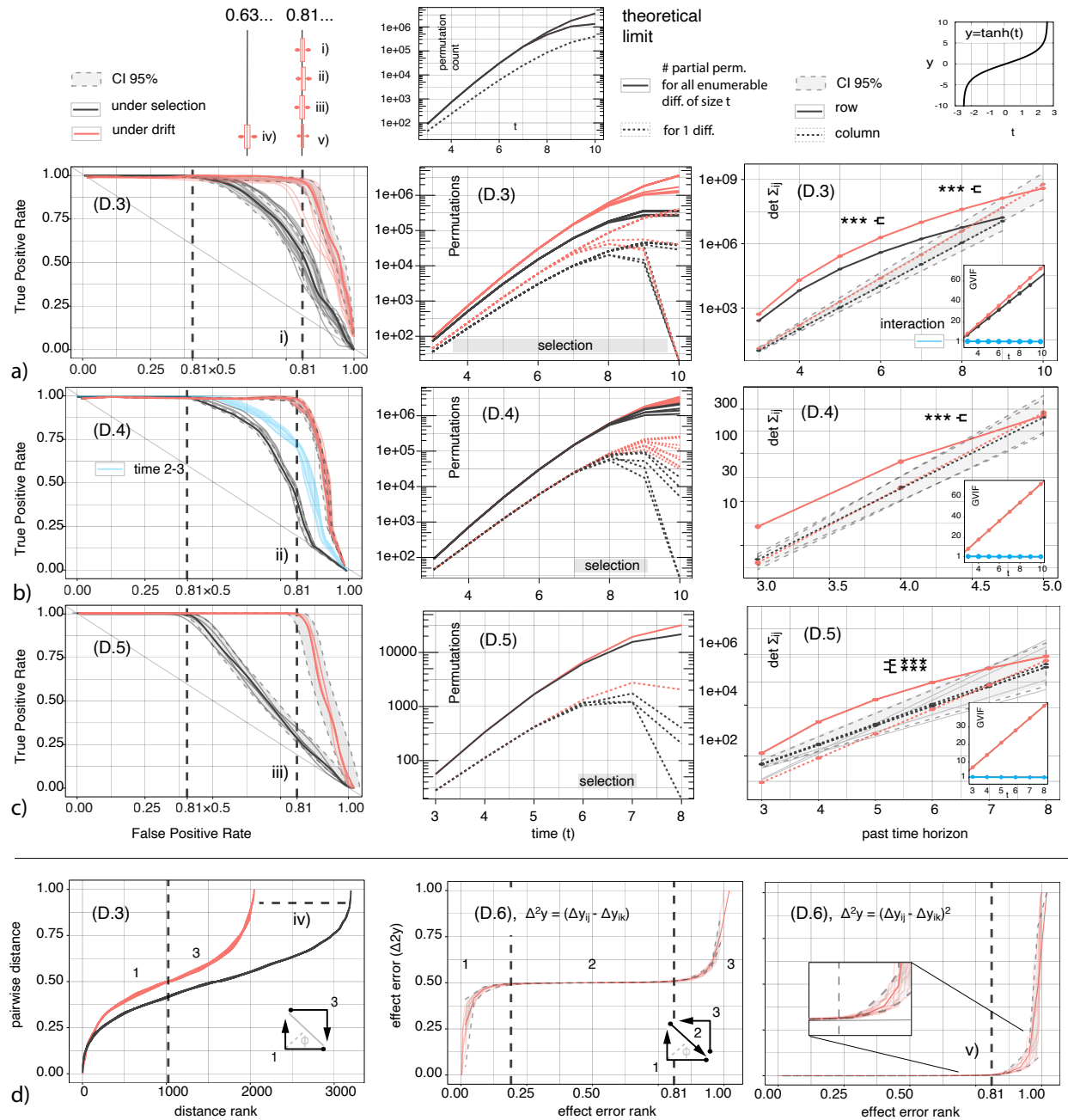


Figure 3 Experimental interventions on selection and effects (fine time-scale).

Experiments over (a) yeast³⁶ (D.3), (b) fly³⁷ (D.4) and (c) E.coli³⁸ (D.5) populations, D.3 and D.5 have populations placed experimentally under selection and D.4 has high selection levels in a single interval, (right) Empirical ROC curves, where dashed lines and box-plot variation (i-iii, top-right panel) show LSM limits, Eq.(2), (middle) theoretical (top panel) and empirical number of (partial) permutations for one and all enumerable differences of size t (y-axis in log-scale), (left) Generalized variance ($\det \Sigma_{ij}$) and their inflations (GVIF, lower panels), (d) (left) spatial distances among all pairs of genes in D.3 follow a \tanh function (top-right panel) and e -sized drift-selection increases (boxplot, iv, top-right panel) as expected by the LSM, (middle-right) experimental effect observations in bi-mutation experiments⁵⁵ (D.6) follow LSM functionals and limits.

ants to become simultaneously balanced (other, purely statistical cases, are discussed in ²⁴). This is seen across all data, D.1-5. By maintaining balance among mutations, increased genetic diversity rates allow effects to remain applicable throughout the diversifying populations, and their full evolutionary trajectories. This is true not only for long time-scale data, but also in fine time-scale experiments.

Combinatorial Enumeration. We now take a purely combinatorial perspective on adaptation, in contrast to the statistical of other results. According to the previous, we can characterize populations by the number of effect observations they generate or enumerate²⁴. A homogeneous population generates none. Systems (2, 3) generate the maximum number of backgrounds under which a (limited) set of variant effects are observed. What we generally consider a genetic difference (e.g., in NT) is a fixed set of t variants that change across a pair of population members. In a partial permutation, while this difference remains fixed, all other $m - t$ factors vary completely. The maximum number of backgrounds for a single difference, (2), of size t thus corresponds to all permutations of m with t positions fixed (i.e., all partial permutations for a single difference). The maximum number of backgrounds for all differences, (3), corresponds to all permutations of 2^m unique differences (i.e., $\max[\pi] = \sum_t^m \binom{m}{t} = 2^m$). The latter is the number of enumerable differences, according to NT, for m sites under drift. Fig.3(a-c, middle-column) show the number of enumerable permutations across time in D.3-5 (y-axis in log-scale). Curves for populations under drift and selection coincide with two combinatorial limits. On the top-left panel is the theoretical limit of permutations (solid line) for differences of size t . Experiment D.3 sustained a selective intervention (stressful, acidic environment) across its 10 time points, while D.4-5 had the intervention concentrated in one point (a natural seasonal change in D.4 and fluorescence-based selection in D.5). These periods are indicated with gray bars in Fig.3(a-c, middle-column). In all cases, the empirical number of permutations had order-of-magnitude increases in the number of partial permutations - this difference sustained throughout the entire experiment in D.3. In fact, systems' empirical number of permutations under drift largely follow the theoretical number of permutations for all differences, Fig.3(a-c, middle-column) - a requirement for type (3) systems. With constant selection (D.3), the number of permutations per each difference under drift coincides with the number of permutations under selection at the end of the experiment. This indicates that the system can observe all permutations, and effect observations, per genetic difference and variant. Experiments with a single intervention, D.4-5, observe a steep increase in the number of partial permutations per difference at the time of intervention ($t = 7$ and $t = 6$) - many replicates going from the limit for a single difference to all differences in this single period. Fewer partial permutations, and steep decreases in the number of partial permutations, are observed in intervals after or under selection. This suggest that evolution is constantly pushing populations against (and is limited by) a combinatorial limit on effect observations and their backgrounds in both cases - with drift associated with limits for more concurrent mutations and genetic differences.

Generalized Variance. The time-extended behavior of systems (2, 3) with rates in Eq.(1) can be visualized with a Latin-Square matrix. Let the first matrix row correspond to a set $\{a, b, c, \dots, [m]\}$ of SNPs at an instant, and columns to environment-population time lags. A population change rate

of $(m - 1/m)$, increases the environment-population lag in one unit of time for all SNPs (thus, as expected, allowing a SNP a to be evaluated against all environmental variations iteratively). This process repeats every m steps, leading to the periodic matrix in Fig.1(d). It was discussed in detail in ²⁴, and is further reviewed in ³⁵. In (2) each environmental background for a SNP corresponds to a cell in the matrix's diagonal, and in (3) to all diagonals (one for each SNP). The Generalized Variance (GV)^{35,58} is the determinant of a population's variance-covariance matrix. Since we defined effect invariance as low variance after all background variation, the GV of the previous matrices, each cell containing an effect observation, can be used as measure of effect invariance. This follows simply from Leibniz permutation-based definition for determinants (i.e., the one taught at the high-school level algebra classes), and the previous definition of effect invariance.

Fig.3(a-c, right-column) show sample variance-covariance determinants calculated independently for populations (row, solid line), $\det \Sigma_{row}$, and time (column, dotted line), $\det \Sigma_{col}$, across experiments. The figure shows that, as in all complete designs, row and column-wise GVs coincide⁵⁹, $\det \Sigma_{row} = \det \Sigma_{col}$. It implies, in turn, that across-diagonal variances between environment and populations coincide in $t_{max} \times t_{max}$ matrices (rightmost dots) - a requirement³⁵ for systems (2, 3). The figure also shows what happens as we reduce the time horizon (x-axis) progressively from t_{max} , from all t_{max} generations until the founder to only 3. This breaks the previous relations, demonstrating how the previous rates generates the populations structures depicted in Fig.1(d) across time, in both evolutionary regimes.

The LSM corresponds to a fully-nested model for effect observations, where we rely not only on main effect estimates, but all interaction effects (thus an ANOVA²⁴ with all combinatorial interactions). In this interpretation, all enumerable interactions correspond to all enumerable effect observation backgrounds. Unbiasedness of effect estimation is therefore associated with the unbiasedness of interaction effects in typical designs. Only by keeping balance among background conditions, we can estimate robustness accurately. As noted by Fox and Monette⁵⁹ (Sect.6), while interaction effects are often ignored in practice, the GV inflation factor (GVIF) is a uniquely suited index to indicate the extent to which population imbalance will compromise interaction effect estimation. In balanced designs, we expect the GVIF of interactions to remain unitary, despite the otherwise large increases in collinearity. This is also shown in Fig.3(a-c, right-column, lower-panels), with interaction GVIFs shown in blue.

Knockout Effect Observations. The previous results showed the consequences of experimental manipulations on evolutionary regimes (same genome, different regimes). As a representational theory of effects, the LSM can also be evaluated with experiments that, instead, manipulate individual variants (and can thus measure, experimentally, their effects on fitness). Before those results, Fig.3(d, left) shows spatial distances among all pairs of genes in D.3 (normalized, in the same chromosome and experimental times). With the LSM assumptions, distance ranks should follow a tanh function³⁵, Fig.3(top-right). Distances among genes are $(1 - 1/e) = 0.63\dots$ times larger under selection, which corresponds to the $(1 - 1/m)^m$ increase in rates illustrated in Fig.1(b,c) and Eq.(2). The figure also shows this scaling factor's variation (iv, box-plot) across all gene pairs

and times.

Temperature-Sensitive (TS) gene knockout experiments intervene on a single gene, adding an allele a , to a genome x_0 . The observed difference in fitness corresponds to a single effect observation, $\Delta y_{ij} = y(x_0 + a) - y(x_0)$. Costanzo et al.⁵⁵ (D.6) measured such effects for all gene pairs (ij) in yeast. Fig.3(d, middle) shows all pairwise differences among effects (normalized, same chromosomes). The plot (of effect differences) follows the same shape as the one for spatial differences, Fig.3(d, left), with an added plateau at 0.5. The plateau corresponds to same, or near, position alleles that are not present in the single and fine experimental time of Fig.3(d, left). It also illustrates effect invariance, and the condition $(\Delta y_{ij} - \Delta y_{ik})^2 = 0$ across all effect differences from a fixed gene i ‡ The plateau is also reminiscent of FGM’s frontier, where many effects take antagonistic values randomly.

We can divide the observation of effects for a given variant in 3 phases (before, after and in the plateau). According to the LSM population-wide representation, the rates in Eq.(2) represents ‘costs’ for increased robustness, or, more precisely, for effect observations under increased genetic backgrounds. Individual effect observations (left) lead to before-after only phases, and across-population observations (middle) to before-plateau-after. This is further illustrated in Fig.3(d, right) which shows *squared* effect differences, and leads to the same 0.8–0.2 limits seen previously, D.1-5. The figure also shows these distinct phases in the previous time-extended matrix representation, Fig.3(d, lower-right diagrams). We can now return to the FGM, whose chief argument was that evolution proceeds by small effect mutations. The argument was also its main source of criticism, starting from Kimura³², who argued, theoretically, for the importance of intermediate effect sizes to adaptation. Contributions from Gillespie, Orr and Gerrish suggested, now including empirical components, that adaptation is characterized by a combination of exponential and small-sized ‘jumps’ in fitness ranks^{60–62}. The previous not only confirms these findings, but also gives them a specific 0.8–0.2 effect size distribution. Additionally, the work here suggests how effects are spatially distributed across the genome, and how their sizes and spatial distributions change under selection.

3 Conclusion

We formulated the hypothesis that adaptation processes systematically amplify the robustness of their mutations. Robustness is highest under specific patterns of lag and synchronicity between systems and their environments. We demonstrated these patterns in the broad time-scale of high-depth genomic datasets, and the fine-scale of multiple barcoding longitudinal experiments (in 6 different ways). Rates in Eq.(2) indicate the number of backgrounds that are observed for each SNP in systems with (2) no variation of other $(m - 1)$ variants, and, (3) full variation of other $(m - 1)$ variants, in the same time interval.

‡where (jk) are all other same-chromosome genes.

The perspective sheds light on fundamental aspects of adaptation, such as its pace, limits and predictability. These limits have implications across the full range of genetics and evolutionary research. The perspective allowed us to present a complete picture of how sets of whole-genomes change in response to environmental changes, and the essential role of standing variation and population structure in adaptation. The picture is one of adaptation as recursive back-and-forths between environments and populations, where rapidly changing environments prompt, in return, the need for systems to generalize gains across these new conditions. We believe this theoretic-empirical perspective could help transform our understanding of evolution, biodiversity maintenance and medical human genomics.

References

1. Zheng, J., Guo, N. & Wagner, A. Selection enhances protein evolvability by increasing mutational robustness and foldability. *Science* **370**, eabb5962 (2020). URL <https://doi.org/10.1126/science.abb5962>.
2. Johnson, M. S., Martsul, A., Kryazhimskiy, S. & Desai, M. M. Higher-fitness yeast genotypes are less robust to deleterious mutations. *Science* **366**, 490–493 (2019). URL <https://doi.org/10.1126/science.aay4199>.
3. Chaturvedi, A. *et al.* Extensive standing genetic variation from a small number of founders enables rapid adaptation in daphnia. *Nature Communications* **12**, 4306 (2021). URL <https://doi.org/10.1038/s41467-021-24581-z>.
4. Hernando-Amado, S., Laborda, P., Valverde, J. & Martínez, J. Mutational background influences *p. aeruginosa* ciprofloxacin resistance evolution but preserves collateral sensitivity robustness. *Proceedings of the National Academy of Sciences* **119**, e2109370119 (2022). URL <https://doi.org/10.1073/pnas.2109370119>.
5. Stewart, B. *et al.* The genetic architecture underlying prey-dependent performance in a microbial predator. *Nature Communications* **13**, 319 (2022). URL <https://doi.org/10.1038/s41467-021-27844-x>.
6. Park, Y., Metzger, B. P. H. & Thornton, J. W. Epistatic drift causes gradual decay of predictability in protein evolution. *Science* **376**, 823–830 (2022). URL <https://doi.org/10.1126/science.abn6895>.
7. Scheuerl, T. *et al.* Bacterial adaptation is constrained in complex communities. *Nature Communications* **11**, 754 (2020). URL <https://doi.org/10.1038/s41467-020-14570-z>.
8. Brennan, R. S., Garrett, A. D., Huber, K. E., Hargarten, H. & Pespeni, M. H. Rare genetic variation and balanced polymorphisms are important for survival in global change conditions. *Proceedings of the Royal Society B: Biological Sciences* **286**, 20190943 (2019). URL <https://doi.org/10.1098/rspb.2019.0943>.

9. Félix, M.-A. & Barkoulas, M. Pervasive robustness in biological systems. *Nature Reviews Genetics* **16**, 483–496 (2015). URL <https://doi.org/10.1038/nrg3949>.
10. Fares, M. A. The origins of mutational robustness. *Trends in Genetics* **31**, 373–381 (2015). URL <https://www.sciencedirect.com/science/article/pii/S016895251500089X>.
11. Draghi, J. A., Parsons, T. L., Wagner, G. P. & Plotkin, J. B. Mutational robustness can facilitate adaptation. *Nature* **463**, 353–355 (2010). URL <https://doi.org/10.1038/nature08694>.
12. Rao, R. & Leibler, S. Evolutionary dynamics, evolutionary forces, and robustness: A nonequilibrium statistical mechanics perspective. *Proceedings of the National Academy of Sciences* **119**, e2112083119 (2022). URL <https://doi.org/10.1073/pnas.2112083119>.
13. LaBar, T. & Adami, C. Evolution of drift robustness in small populations. *Nature Communications* **8**, 1012 (2017). URL <https://doi.org/10.1038/s41467-017-01003-7>.
14. Wilke, C. O., Wang, J. L., Ofria, C., Lenski, R. E. & Adami, C. Evolution of digital organisms at high mutation rates leads to survival of the flattest. *Nature* **412**, 331–333 (2001). URL <https://doi.org/10.1038/35085569>.
15. Krakauer, D. C. & Plotkin, J. B. Redundancy, antiredundancy, and the robustness of genomes. *Proceedings of the National Academy of Sciences* **99**, 1405–1409 (2002). URL <https://doi.org/10.1073/pnas.032668599>.
16. van Nimwegen, E., Crutchfield, J. P. & Huynen, M. Neutral evolution of mutational robustness. *Proceedings of the National Academy of Sciences* **96**, 9716–9720 (1999). URL <https://doi.org/10.1073/pnas.96.17.9716>.
17. Allen, B. *et al.* Evolutionary dynamics on any population structure. *Nature* **544** (2017).
18. Pavlogiannis, A., Tkadlec, J., Chatterjee, K. & Nowak, M. A. Construction of arbitrarily strong amplifiers of natural selection using evolutionary graph theory. *Communications biology* **1**, 71 (2018).
19. Lieberman, E., Hauert, C. & Nowak, M. A. Evolutionary dynamics on graphs. *Nature* **433**, 312 (2005).
20. Fisher, S., Ronald Aylmer. *The genetical theory of natural selection* (Clarendon Press, Oxford, 1930). URL <https://www.biodiversitylibrary.org/item/69976>.
21. Tenaillon, O. The utility of fisher’s geometric model in evolutionary genetics. *Annual Review of Ecology, Evolution, and Systematics* **45**, 179–201 (2014). URL <https://doi.org/10.1146/annurev-ecolsys-120213-091846>.

22. Orr, H. A. Theories of adaptation: what they do and don't say. *Genetica* **123**, 3–13 (2005). URL <https://doi.org/10.1007/s10709-004-2702-3>.
23. Montgomery, D. C. *Design and analysis of experiments* (John Wiley, New York, 2001).
24. Ribeiro, A. F. & Nonato, L. G. The external validity of combinatorial samples and populations (2021, Under Review). URL <https://arxiv.org/abs/2108.04376>.
25. Breen, M. S., Kemena, C., Vlasov, P. K., Notredame, C. & Kondrashov, F. A. Epistasis as the primary factor in molecular evolution. *Nature* **490**, 535–538 (2012). URL <https://doi.org/10.1038/nature11510>.
26. Kryazhimskiy, S., Rice, D. P., Jerison, E. R. & Desai, M. M. Global epistasis makes adaptation predictable despite sequence-level stochasticity. *Science* **344**, 1519–1522 (2014). URL <https://doi.org/10.1126/science.1250939>.
27. Boyer, C. *A History of Mathematics* (Wiley, 1968). URL <https://books.google.com.br/books?id=1ZDuAAAAMAAJ>.
28. Gazale, M. J. *Gnomon: from pharaohs to fractals* (Princeton University Press, Princeton, N.J, 1999).
29. Auton, A. *et al.* A global reference for human genetic variation. *Nature* **526**, 68–74 (2015). URL <https://doi.org/10.1038/nature15393>.
30. Halldorsson, B. V. *et al.* The sequences of 150,119 genomes in the uk biobank. *Nature* **607**, 732–740 (2022). URL <https://doi.org/10.1038/s41586-022-04965-x>.
31. Watterson, G. A. On the number of segregating sites in genetical models without recombination. *Theoretical Population Biology* **7**, 256–276 (1975).
32. Kimura, M. *The Neutral Theory of Molecular Evolution* (Cambridge University Press, Cambridge, 1983). URL <https://www.cambridge.org/core/books/neutral-theory-of-molecular-evolution/0FF60E9F47915B17FFA2620C49400632>.
33. Tajima, F. Evolutionary relationship of dna sequences in finite populations. *Genetics* **105**, 437 (1983).
34. McCandlish, D. M. & Stoltzfus, A. Modeling evolution using the probability of fixation: History and implications. *The Quarterly Review of Biology* **89**, 225–252 (2014). URL <https://doi.org/10.1086/677571>.
35. Supporting material (2022).
36. Wang, X., Zorraquino, V., Kim, M., Tsoukalas, A. & Tagkopoulos, I. Predicting the evolution of escherichia coli by a data-driven approach. *Nature Communications* **9**, 3562 (2018). URL <https://doi.org/10.1038/s41467-018-05807-z>.

37. Nosil, P., Flaxman, S. M., Feder, J. L. & Gompert, Z. Increasing our ability to predict contemporary evolution. *Nature Communications* **11**, 5592 (2020). URL <https://doi.org/10.1038/s41467-020-19437-x>.
38. Nosil, P. *et al.* Natural selection and the predictability of evolution in timema stick insects. *Science* **359**, 765–770 (2018). URL <https://doi.org/10.1126/science.aap9125>.
39. Weinberger, E. D. Fourier and Taylor series on fitness landscapes. *Biological Cybernetics* **65**, 321–330 (1991). URL <https://doi.org/10.1007/BF00216965>.
40. Poelwijk, F. J., Krishna, V. & Ranganathan, R. The context-dependence of mutations: A linkage of formalisms. *PLOS Computational Biology* **12**, e1004771– (2016). URL <https://doi.org/10.1371/journal.pcbi.1004771>.
41. Henn, B. M., Cavalli-Sforza, L. L. & Feldman, M. W. The great human expansion. *Proceedings of the National Academy of Sciences* **109**, 17758 (2012).
42. Amos, W. & Hoffman, J. I. Evidence that two main bottleneck events shaped modern human genetic diversity. *Proceedings of the Royal Society B: Biological Sciences* **277**, 131–137 (2010). URL <https://doi.org/10.1098/rspb.2009.1473>.
43. Carlson, C. S. *et al.* Genomic regions exhibiting positive selection identified from dense genotype data. *Genome Res* **15**, 1553–1565 (2005).
44. Hawks, J., Wang, E. T., Cochran, G. M., Harpending, H. C. & Moyzis, R. K. Recent acceleration of human adaptive evolution. *Proc Natl Acad Sci U S A* **104**, 20753–20758 (2007).
45. Kayser, M., Brauer, S. & Stoneking, M. A genome scan to detect candidate regions influenced by local natural selection in human populations. *Mol Biol Evol* **20**, 893–900 (2003).
46. Sabeti, P. C. *et al.* Genome-wide detection and characterization of positive selection in human populations. *Nature* **449**, 913–918 (2007).
47. Courtiol, A. *et al.* The demographic transition influences variance in fitness and selection on height and BMI in rural Gambia. *Current Biology* **23**, 884–889 (2013). URL <https://www.sciencedirect.com/science/article/pii/S0960982213004144>.
48. Akey, J. M. *et al.* Population history and natural selection shape patterns of genetic variation in 132 genes. *PLoS Biol* **2**, e286 (2004).
49. Ghosh, S. *Asymptotics, Nonparametrics, and Time Series (Chapter 2)* (CRC Press, Boca Raton, FL, 1999). URL <https://www.taylorfrancis.com/books/9781482269772>.
50. Hurd, H. L. & Gerr, N. L. Graphical methods for determining the presence of periodic correlation. *Journal of Time Series Analysis* **12**, 337–350 (1991). URL <https://doi.org/10.1111/j.1467-9892.1991.tb00088.x>.

51. Todesco, M. *et al.* Massive haplotypes underlie ecotypic differentiation in sunflowers. *Nature* **584**, 602–607 (2020). URL <https://doi.org/10.1038/s41586-020-2467-6>.
52. Gabriel, S. B. *et al.* The structure of haplotype blocks in the human genome. *Science* **296**, 2225–2229 (2002). URL <https://doi.org/10.1126/science.1069424>.
53. Frisse, L. *et al.* Gene conversion and different population histories may explain the contrast between polymorphism and linkage disequilibrium levels. *The American Journal of Human Genetics* **69**, 831–843 (2001). URL <https://doi.org/10.1086/323612>.
54. Reich, D. E. *et al.* Linkage disequilibrium in the human genome. *Nature* **411**, 199–204 (2001). URL <https://doi.org/10.1038/35075590>.
55. Costanzo, M. *et al.* A global genetic interaction network maps a wiring diagram of cellular function. *Science* **353**, aaf1420 (2016). URL <https://doi.org/10.1126/science.aaf1420>.
56. Nguyen Ba, A. N. *et al.* High-resolution lineage tracking reveals travelling wave of adaptation in laboratory yeast. *Nature* **575**, 494–499 (2019). URL <https://doi.org/10.1038/s41586-019-1749-3>.
57. Rudman, S. M. *et al.* Direct observation of adaptive tracking on ecological time scales in drosophila. *Science* **375**, eabj7484. URL <https://doi.org/10.1126/science.abj7484>.
58. Sen Gupta, A. *Generalized Variance* (2006). URL <https://doi.org/10.1002/0471667196.ess6053.pub2>.
59. Fox, J. & Monette, G. Generalized collinearity diagnostics. *Journal of the American Statistical Association* **87**, 178–183 (1992). URL <https://www.tandfonline.com/doi/abs/10.1080/01621459.1992.10475190>.
60. Gerrish, P. The rhythm of microbial adaptation. *Nature* **413**, 299–302 (2001). URL <https://doi.org/10.1038/35095046>.
61. Orr, H. A. The population genetics of adaptation: The adaptation of dna sequences. *Evolution* **56**, 1317–1330 (2002). URL <https://doi.org/10.1111/j.0014-3820.2002.tb01446.x>.
62. Rozen, D. E., de Visser, J. A. G. M. & Gerrish, P. J. Fitness effects of fixed beneficial mutations in microbial populations. *Current Biology* **12**, 1040–1045 (2002). URL <https://www.sciencedirect.com/science/article/pii/S0960982202008965>.